3rd Specialty Conference on Material Engineering & Applied Mechanics
3e Conférence spécialisée sur le génie des matériaux et mécanique appliquée

Montréal, Québec
May 29 to June 1, 2013 / *29 mai au 1 juin 2013*

Modelling of Steel Behaviour for Monotonic and Cyclic Loading

Z. Wen[1], H. Khoo[2]
[1]Architectural Design and Research Institute of Tongji University, Shanghai, China.
[2]Department of Civil and Environmental Engineering, Carleton University, Ottawa, Ontario.

Abstract: An accurate modelling of the material behavior is important in the design and analysis of a structure. The combined isotropic and kinematic hardening material model proposed by Chaboche has been one of the models that is widely used in the numerical modelling to simulate the response of steel under cyclic loading. A combined experimental and numerical study has been carried to develop a procedure to systematically calculate the parameters for the model that can predict the material response under both monotonic and cyclic loading. Nineteen straight and notched round specimens of ASTM A572 Grade 50 steel were tested under monotonic and cyclic loading until fracture. The cyclic tests were carried out at various strain ranges. A systematic procedure that enables the calculation of the parameters for the material model that are equally applicable for monotonic and cyclic loading has been developed and are presented. Numerical simulations with these parameters have been found to be in good agreement with the measured stress-strain curves of the round specimen tests. Good agreement has also been found between the test and predicted instance of fracture of the specimen using a variation of the continuum damage mechanics fracture criteria by Lemaitre.

1 Introduction

The performance of structures under any loading condition is greatly dependent on the material behaviour. An accurate modelling of the material behavior is important in the design and analysis of a structure especially in assessing the performance a structure to withstand seismic load. The combined isotropic and kinematic hardening material model proposed by Chaboche (1986) has been one of the models that is widely used in the numerical modelling to simulate the response of steel under cyclic loading. In steel structures, ductile fracture may occur due to low-cycle fatigue and overload. However, parameters for the material model used in most numerical simulations (Kanvinde and Deierlein 2004) carried out to predict fracture for low-cycle fatigue were different from that for predicting fracture under monotonic loading. Since the loading type that leads to fracture in a real situation is not known a priori, only a single set of material model parameters have to be used in a general numerical simulation to model both monotonic and cyclic loading. Thus, the challenge is to determine a single set of parameters that can reasonably model the behaviour for both monotonic and cyclic loading until fracture.

2 Background

2.1 Combined Isotropic and Kinematic Hardening Plasticity Material Model

There are two basic work hardening rules that are widely used in describing the plastic behaviour of steel (metals): isotropic hardening and kinematic hardening. Isotropic hardening occurs when the yield surface expands uniformly in the stress space during plastic deformation. In kinematic hardening, the yield surface does not change its form and orientation but translates in the stress space similar to a rigid body

translation. When combining isotropic and kinematic hardening rules to describe the plastic behaviour, the yield surface translates in the stress space as well as expanding or contracting in its size. Some basic concepts of plasticity are introduced below to help facilitate the discussion. The yield function is given by

[1] $$f(\sigma_{ij} - \alpha_{ij}, \kappa) = 0$$

where σ_{ij} is the stress tensor, α_{ij} is the backstress tensor and κ is a scalar that defines the size of the yield surface. For metals, von Mises yield criterion for isotropic material that combines isotropic and kinematic hardening can be expressed as

[2] $$(S_{ij} - \alpha_{ij})(S_{ij} - \alpha_{ij}) - \kappa^2 = 0$$

where S_{ij} is the deviatoric stress tensor. The plastic deformation of metals is normally assumed to follow the associated flow rule, which is given by

[3] $$d\varepsilon_{ij}^{p} = \frac{\partial f}{\partial \sigma_{ij}} d\lambda ,$$

where $d\varepsilon_{ij}^{p}$ is the change in the plastic strain tensor and $d\lambda$ is a constant of proportionality with the equivalent plastic strain increment defined as

[4] $$d\varepsilon_{eq}^{p} = \sqrt{\frac{2}{3} d\varepsilon_{ij}^{p} d\varepsilon_{ij}^{p}} .$$

Similarly, the equivalent stress associated with plastic deformation can be defined as

[5] $$\sigma_{eq} = \sqrt{\frac{3}{2} S_{ij} S_{ij}} .$$

Chaboche (1986) proposed a combined isotropic and nonlinear kinematic hardening model with multiple backstress evolution terms that was derived from the model by Armstrong and Frederick (1966). The backstress evolution for the model by Chaboche can be expressed as

[6] $$d^{k}\alpha_{ij} = C_k d\varepsilon_{ij}^{p} - \gamma_k \alpha_{ij} d\varepsilon_{eq}^{p} \text{ and}$$

[7] $$\alpha_{ij} = \sum {}^{k}\alpha_{ij}$$

with k denotes the backstress tensor α_{ij}, material constants C and γ for the k kinematic hardening term.

2.2 Fracture Criteria

There have a number of criteria proposed to predict fracture of steel. Huang and Mahin (2008) has adopted the fracture criteria based on continuum damage mechanics developed by Lemaitre (1985) in their study. In the present study, a variation of the criteria and damage evolution by Huang and Mahin has been adopted to predict fracture of the specimen. The damage evolution adopted in this study can be expressed as

[8] $$dD = \begin{cases} (cy)^{m} d\varepsilon_{eq}^{p} & \text{for } \dfrac{\sigma_m}{\sigma_{eq}} > -\dfrac{1}{3} \\ 0 & \text{otherwise} \end{cases}, \text{ with}$$

[9] $$y = \frac{\sigma_{eq}^{\ 2}}{2E}\left[\frac{2}{3}(1+\nu)+3(1-2\nu)\left(\frac{\sigma_m}{\sigma_{eq}}\right)^q\right]$$

where D is the damage, c, m and q are material constants, σ_m is the hydrostatic or mean stress, E is the elastic modulus and ν is the Poisson's ratio. Fracture is assumed to occur when the damage D reaches a critical limit D_c. Unlike the criteria by Huang and Mahin, the exponent q on stress triaxiality, σ_m/σ_{eq}, is allowed to vary, and the state of damage D is assumed to be uncoupled from the material constitutive relationship. Thus, the state of damage D does not appear in Eq. [9] for the expression associated with the strain energy density.

3 Test Program

A total of thirty nine specimens of ASTM A572 Grade 50 and CSA G40.20/21 Grade 300W steel were tested by Wen (2012). Only results of nineteen specimens of ASTM A572 Grade 50 steel are discussed in this paper. Kanvinde and Deierlein (2004) have conducted many ultra low-cycle fatigue tests on Grade 50 (F_y = 345 MPa) and higher strength steels. The test program by Kanvinde and Deierlein has been used as a reference in designing the test matrix for the present study.

Effects of mean stress, strain range and loading sequence are investigated in the current test program. Tests were carried out with different mean to effective stress ratio (σ_m/σ_{eq}) by using specimens with straight and notched profiles. The profile of the straight and notched specimens are shown in Figs.1 to 3.Three loading sequences up to fracture consist of monotonic tension, cyclic loading followed by tension, and cyclic loading only were considered. Specimens were subjected to both a large strain range but a small number of up to 20 cycles to fracture similar to the tests by Kanvinde and Deierlein and as well as subjected to a smaller strain range but a larger number of loading cycle to fracture. The test matrix is listed in Table 1.

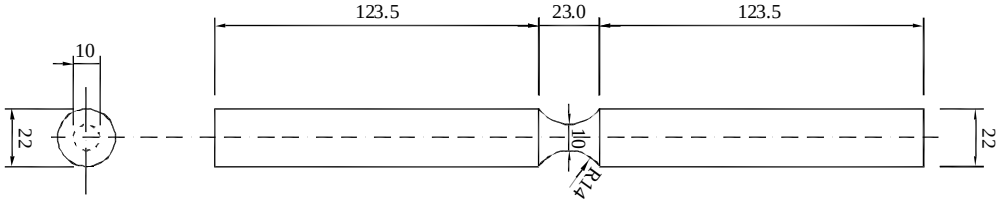

Figure 1: Notched specimen profile A (D10R14N) with dimensions in mm

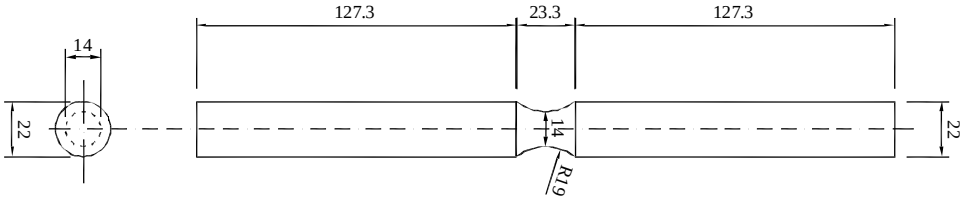

Figure 2: Notched specimen profile B (D14R19N) with dimensions in mm

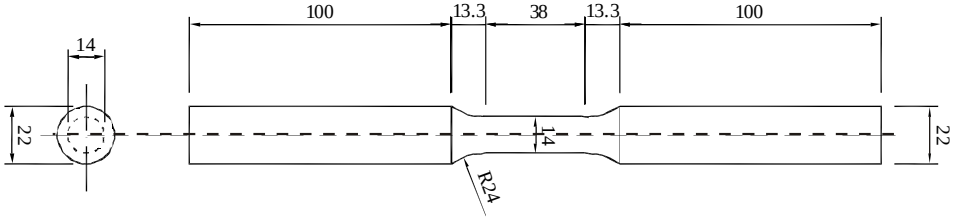

Figure 3: Straight specimen profile D (D14R24U) with dimensions in mm

Table 1. Test matrix

Specimen	Profile	Test type	Nominal engineering cyclic strain range	Nominal true cyclic strain range
ADMa	D14R24U	Monotonic test	–	–
ADMb	D14R24U	Monotonic test	–	–
AAMa	D10R14N	Monotonic test	–	–
AAMb	D10R14N	Monotonic test	–	–
ABM	D14R19N	Monotonic test	–	–
ADC20202	D14R24U	20 cycles, pull to failure	±2%	±2%
ADC40101	D14R24U	40 cycles, pull to failure	±1%	±1%
ADC40102	D14R24U	40 cycles, pull to failure	-2% to 1%	-2% to 1%
ADC40202	D14R24U	40 cycles, pull to failure	±2%	±2%
ADCR0201	D14R24U	30 cycles, pull to failure	±2%, ±1%	±2%, ±1% [1]
AAC20404	D10R14N	20 cycles, pull to failure	±0.6%	±4%
ABC20404	D14R19N	20 cycles, pull to failure	±0.9%	±4%
AAC70404	D10R14N	70 cycles, pull to failure	±0.6%	±4%
ABC70404	D14R19N	70 cycles, pull to failure	±0.9%	±4%
AACF1212	D10R14N	Cycle to failure	-1.8% to 1.65%	±12%
ABCF1212	D14R19N	Cycle to failure	-2.8% to 2.3%	±12%
AACF3010	D10R14N	Cycle to failure	-1.5% to 3.67%	-10% to 30%
ABCF3010	D14R19N	Cycle to failure	-2.3% to 5%	-10% to 30%
AACR0804	D10R14N	Cycle to failure	±1.2%, ±0.6%	±8%, ±4% [2]

Notes:
[1] First subjected to 10 cycles of loading between strain range of -2% to +2%, then subjected to 20 cycles of loading between strain range of -1% to +1% before being pulled to failure in tension.
[2] First subjected to 8 cycles of loading between nominal true strain range of -8% to +8%, then subjected to cyclic loading between nominal true strain range of -4% to +4% until failure.

4 Calibration of Parameters for Material Model

For the mixed-mode hardening model proposed by Chaboche (1986), the equivalent flow stress can be expressed as

[10] $$\sigma^y = \sqrt{\frac{3}{2} S_{ij} S_{ij}} \quad \text{and}$$

[11] $$\sigma^0 = \sqrt{\frac{3}{2} (S_{ij} - \alpha_{ij})(S_{ij} - \alpha_{ij})}$$

for the size of the yield surface based on von Mises yield criterion. Under uniaxial tension loading, the flow stress reduces to

[12] $$\sigma^y = |\sigma_{11}| = \sigma^0 + \alpha \quad \text{and the backstress}$$

[13] $$\alpha = \text{sgn}(\alpha_{11}) \sqrt{\frac{3}{2} \alpha_{ij} \alpha_{ij}}$$

where σ_{11} and α_{11} are the normal stress and backstress in the loading direction, sgn(α_{11}) is 1 when α_{11} is positive and -1 when α_{11} is negative.

4.1 Calibration of Parameters for Flow Stress Equation

For a standard straight specimen, the stress and strain are uniform across the reduced section of the specimen before necking occurs. The true stress σ_t for a straight specimen can be taken

[14] $$\sigma_t = \frac{F}{A} = \frac{F}{A_0}\left(\frac{A_0}{A}\right) = \sigma_e\left(\frac{A_0}{A}\right) \text{ and}$$

approximated as $\sigma_e(1+\varepsilon_e)$ where F is the load, A is the current cross-sectional area, A_0 is the undeformed cross-sectional area, σ_e is the engineering stress and ε_e is the engineering strain. The true strain is given by

[15] $$\varepsilon_t = \ln(1+\varepsilon_e) \text{, and approximated as}$$

[16] $$\approx \ln\left(\frac{A_0}{A}\right) \text{, with}$$

[17] $$\varepsilon_t^p = \varepsilon_t - \frac{\sigma_t}{E}$$

for the true plastic strain. These equations are valid up to the peak load point before necking occurs. Due to the non-uniform stress and strain distribution at the necking region, only Eqs. [14], [16] and [17] can be used as the approximate calculations after necking has started. Chen (2010) has proposed using an empirical equation to estimate the flow stress versus equivalent plastic strain curve after the peak load directly from the test data. After necking has occurred, the true flow stress can be corrected according to the equation to be

[18] $$\sigma_t^{cor} = 0.5\sigma_t^{avg}\left(1+\sqrt{\frac{A}{A_{peak}}}\right)$$

where A_{peak} is the cross-sectional area at peak stress, σ_t^{avg} is the average true flow stress given by Eq. [14]. However, an equation to describe the flow stress in terms of plastic strain has to be used in order be

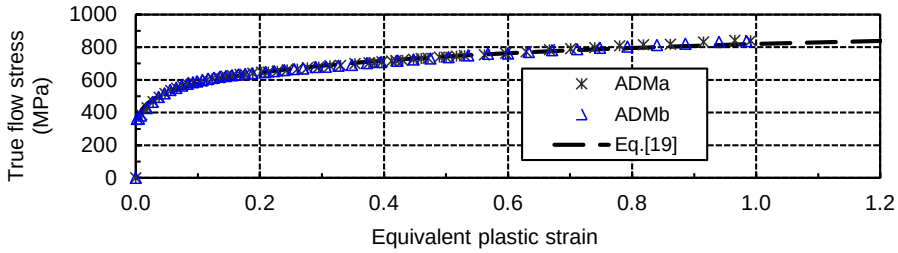

Figure 4: Curve fitting of the flow stress versus equivalent plastic strain data of straight specimens

able to define the flow stress beyond the strain that necking occurs under uniaxial monotonic tension loading. A modified equation proposed by Chinh et al. (2004)

[19] $$\sigma^y = \sigma_0^y + \sigma_\infty^y\left[1 - e^{-b\left(\varepsilon^p - \varepsilon_0^p\right)^n}\right]$$

where σ_0^y is the initial flow stress, σ_∞^y is the maximum additional flow stress, ε^p is the plastic strain, ε_0^p is the plastic strain at the start of strain hardening, b and n are material constants can be used to describe on the flow stress in terms of plastic strain. Parameters of Eq. [19] for a material can be determined

through least-square fitting of the measured flow stress vs. plastic strain calculated using Eqs. [14] to [18] for a straight profile specimen under uniaxial monotonic tension loading. Figures 4 and 5 show results of curve fitting of Eq. [19] and the predicted load (stress) vs. deformation of straight profile specimen tests using the calculated parameters. All numerical simulations in the present study were carried out using finite element analyses package ABAQUS (Simulia 2009).

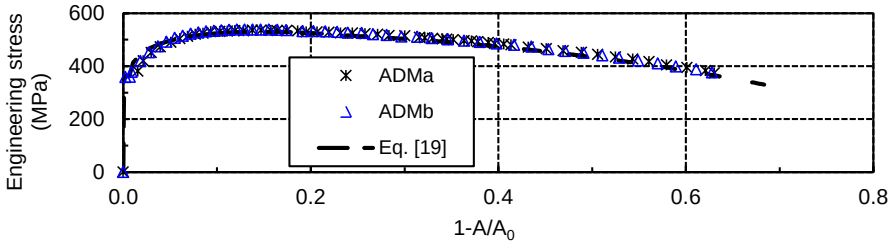

Figure 5: Test and predicted engineering stress versus deformation curves for straight specimens

4.2 Calibration of Parameters for Combined Isotropic and Kinematic Hardening Model

Parameters for kinematic hardening C and γ, and σ^o vs. ε^p relationship have to be defined in order to carry out the numerical simulation using the model by Chaboche (1986). Figure 6 shows the relationship between various stress components under monotonic uniaxial tension loading according to Eq. [12]. If parameters for kinematic hardening C and γ are known, σ^o vs. ε^p relationship can be calculated according to the relationship between various stress components shown in Fig. 6 by substracting the backstress α calculated using C and γ from the flow stress in Fig. 4 that has been established with Eq. [19]. The backstress for each kinematic hardening term under uniaxial monotonic loading is given by

$$[20] \qquad {}^{k}\alpha = \frac{C_k}{\gamma_k}\left(1 - e^{-\gamma_k \varepsilon^p}\right).$$

From results of the tests, it can be expected that structural steel can have a large accumulated plastic strain under cyclic loading before fracture occurs. For this reason, the calibration of the parameters for the kinematic hardening should consider the behaviour at both small and large strains.

For the calibration at small strain, data from a stabilized cycle under uniaxial cyclic loading such as specimen ADC40202, can be used to approximate the backstress by taking σ^o in Eq. [12] to be the saturated yield stress σ_s^0. Only one branch of the stabilized stress-strain curve due to either tension or compression is needed for the calibration. Using the tension branch, the assumed static true stress versus true plastic strain curve used in the calibration is shown in Fig. 7. For calibration purposes, the start of the assumed curve is taken as twice the assumed saturated yield stress ($2\,\sigma_s^0$) above the point at the beginning of the tension branch. It is taken to be a constant until it is exceeded by the test data. Since the flow stress is a summation of yield stress and backstress, the backstress therefore can be obtained by subtracting the assumed saturated yield stress from the static true stress versus true plastic strain curve. Plotting relative to the start of the tension branch, Fig. 8 shows the calculated backstress at the selected 15 evenly spaced data points along the strain range used in the calibration at the 20th cycle of ADC40202 for σ_s^0 = 464 MPa. The backstress in Fig. 8 can be expressed according to the evolution in Eq. [6] as

$$[21] \qquad {}^{k}\alpha = -\frac{C_k}{\gamma_k}\frac{[1 - e^{(-\gamma_k \Delta\varepsilon^p)}]}{[1 + e^{(-\gamma_k \Delta\varepsilon^p)}]} e^{(-\gamma_k \varepsilon^p)} + \frac{C_k}{\gamma_k}\left[1 - e^{(-\gamma_k \varepsilon^p)}\right]$$

where $\Delta\varepsilon^p$ is the plastic strain range and ε^p is the incremental plastic strain from the beginning of tension branch.

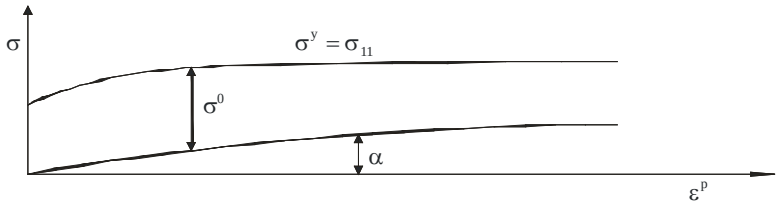

Figure 6: Relationship between various stress components under monotonic uniaxial tension loading

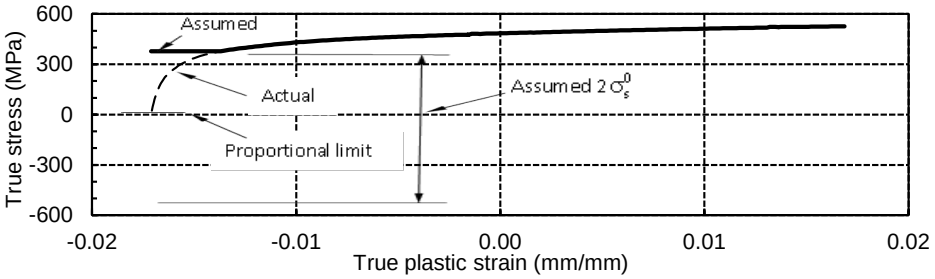

Figure 7: Assumed saturated true stress vs. true plastic strain curve, tension branch ADC40202 cycle #20

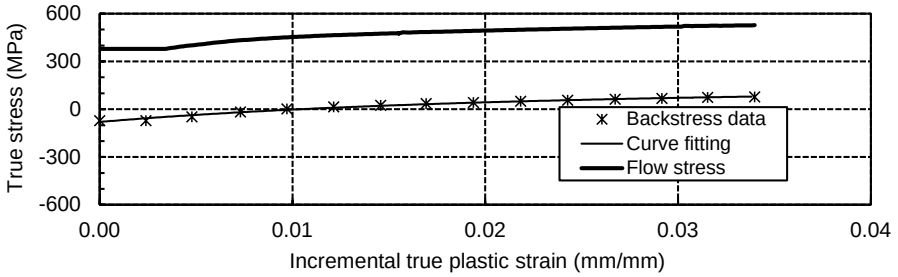

Figure 8: Curve fitting of backstress for small strain, tension branch ADC40202 cycle #20, σ_s^0 = 464 MPa

The data used in calibrating the kinematic hardening parameters at large strain range curve can be generated from the equation describing the flow stress and the assumed saturated yield stress. Based on the parameters solved for Eq. [19] and the assumed saturated yield stress, the backstress versus plastic strain data can be calculated using Eq. [12]. From results of the cyclic test of a straight specimen at ±2% strain, the stress-strain curve is close to be stabilized only after a few cycles of loading. Thus, for the purpose of calibrating kinematic hardening parameters at large strain, the yield stress can be assumed to be saturated at a strain of 0.2 when generating the data points for the calibration. It has been found that using of data points up to the strain of 10 in the calibration is sufficient to ensure that the stress generated with the calibrated hardening parameters to be constant after the strain of 10. Figure 9 shows the backstress versus plastic strain curve used in calibrating the kinematic hardening parameters based on Eq. [20] for σ_s^0 = 464 MPa and $\Delta\sigma_s^0$ = 14 MPa, where 30 evenly spaced data points have been selected from the strain range of 0.2 to 10 as compared to the 15 data points for small strain. The 2 to 1 ratio in the number of data points for large strain versus small strain has been found to give a good result in the calibration. Although the stress versus strain curve of ADC40202 may appear to be stabilized at the 20th cycle, the yield stress at the 20th cycle may actually be different from the final saturated yield stress at a very large strain. For this reason, the addition of $\Delta\sigma_s^0$ to σ_s^0 as the assumed saturated yield stress to generate large strain calibration data allows two assumed yield stresses to be used in calculating the backstress data in least-square fitting to obtain the kinematic hardening parameters. The kinematic

hardening parameters C_k and γ_k are determined by least-square fitting of Eq. [21] through the backstress in Fig. 8 and Eq. [20] through the backstress in Fig. 9 concurrently. Numerical simulations using the σ^o vs. ε^p relationship established with these kinematic hardening parameters are compared to the load (stress) vs. deformation (strain) curve of the cyclic notched specimen test, ABC20404, to obtain the optimum kinematic hardening parameters. Values of σ_s^0 and $\Delta\sigma_s^0$ are adjusted until a good match between the test and predicted load (stress) vs. deformation (strain) curve of ABC20404 has been achieved.

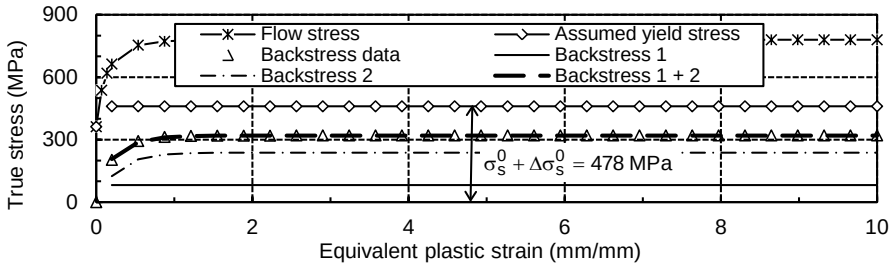

Figure 9: Curve fitting of backstress for large strain with σ_s^0 = 464 MPa and $\Delta\sigma_s^0$ = 14 MPa

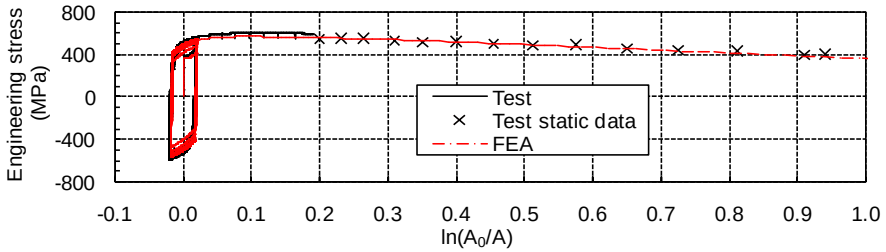

Figure 10: Test and predicted stress versus deformation curves for straight specimen ADC40202

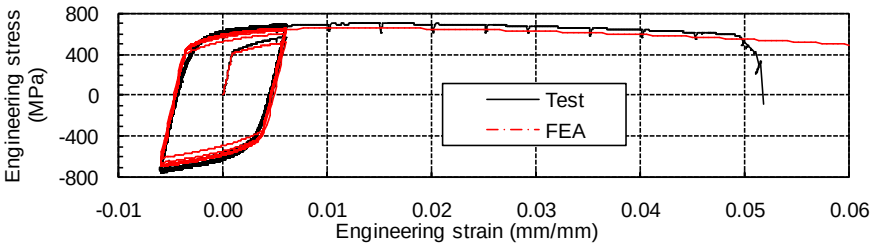

Figure 11: Test and predicted stress versus strain curves for notched specimen AAC70404

Using two kinematic hardening terms, the optimum hardening parameters are obtained with σ_s^0 = 464 MPa and $\Delta\sigma_s^0$ = 14 MPa. It has been found that numerical simulations with one kinematic hardening term could not closely predict results of all tests. With an assumed Poisson's ratio ν = 0.3, the measured elastic modulus E = 205600 MPa, σ_0^y = 362 MPa and ε_0^p = 0.0053, the rest of the parameters for the hardening model have been determined to be σ_∞^y = 417 MPa, n = 0.77, b = 4.53, C_1 = 3625 MPa, γ_1 = 39.46, C_2 = 711 MPa and γ_2 = 3.39. Curve fitting used in obtaining the optimum hardening parameters are shown in Figs. 8 and 9. Using these parameters, numerical simulations were carried out for all other tests. Comparisons of the test and predicted load (stress) vs. deformation (strain) curve for some of the tests are shown in Figs. 5, 10 and 11. There is good agreement between the test and predicted load (stress) vs. deformation (strain) curves for different specimen profiles and loading.

5 Fracture Prediction

Using results of numerical simulations in Section 4.2, a simple trapezoidal integration rule has been employed to calculate the damage evolution of Eq. [8] as

$$[22] \qquad \int_0^{\varepsilon_{eq}^{pf}} f(\sigma) d\varepsilon_{eq}^{p} \approx \sum_{i=1}^{m} \left[\frac{f(\sigma)_{i-1} + f(\sigma)_i}{2} \right] \Delta\varepsilon_{eq}^{p}$$

where i is the current time increment step of the total m increment steps, $f(\sigma)$ is the damage evolution function of damage criterion, $\Delta\varepsilon_{eq}^{p}$ is the change in the equivalent plastic strain at the increment step i, ε_{eq}^{pf} is the equivalent plastic strain at fracture. The damage measurement at fracture D_c for each

Table 2. Test and predicted point of fracture, c = 1, m = 3.07, k = 1.44, $\overline{D_c}$ = 9.95

Specimen	Test type / fracture	Damage at fracture	d_p/d_f	$(d_0-d_p)/(d_0-d_f)$	Predicted fracture cycle	ε_{af}	ε_{ap}	$\varepsilon_{af}/\varepsilon_{ap}$
ADMa	Monotonic	10.53	1.01	0.98	—	—	—	—
ADMb	Monotonic	10.33	1.01	0.99	—	—	—	—
AAMa	Monotonic	7.62	0.96	1.09	—	0.070	0.073	1.04
AAMb	Monotonic	8.21	0.97	1.06	—	0.070	0.073	1.04
ABM	Monotonic	6.66	0.95	1.14	—	0.094	0.102	1.09
ADC20202	20 cycles+	10.68	1.01	0.98	20+	—	—	—
ADC40101	40 cycles+	8.49	0.97	1.05	40+	—	—	—
ADC40102	40 cycles+	9.83	1.00	1.00	40+	—	—	—
ADC40202	40 cycles+	10.11	1.00	1.00	40+	—	—	—
ADCR0201	30 cycles+	10.39	1.01	0.99	30+	—	—	—
AAC20404	20 cycles+	11.02	1.02	0.95	20+	0.544	0.535	0.98
ABC20404	20 cycles+	12.27	1.04	0.89	20+	0.805	0.794	0.99
AAC70404	70 cycles+	14.42	1.25	0.04	70	1.729	1.675	0.97
ABC70404	70 cycles+	12.35	1.08	0.17	62	2.554	2.226	0.87
AACF1212	9 cycles	9.36	0.95	2.17	9	0.621	0.633	1.02
ABCF1212	7 cycles	9.02	1.03	0.73	8	0.734	0.822	1.12
AACF3010	3 cycles	8.73	0.95	1.22	3	0.339	0.346	1.02
ABCF3010	3 cycles	7.81	0.88	2.17	3	0.448	0.478	1.07
AACR0804	48 cycles	9.95	1.05	-0.07	49	1.350	1.364	1.01

specimen is calculated with Eq. [22] up to the cross-sectional reduction equal to that of the test at fracture. The arithmetical average of the damage at fracture $\overline{D_c}$ of all the test specimens is regarded as the damage limit. Parameters m and q in Eqs. [8] and [9] are adjusted until the error ER in the predicted damage at fracture is minimized according to

$$[23] \qquad ER = \sum_{j=1}^{p} \left| \frac{(D_c)_j - \overline{D_c}}{\overline{D_c}} \right|$$

where j is the specimen number for a total of p specimens. The predicted diameter and/or loading cycle at fracture for each specimen is assumed to occur when the accumulated damage reaches $\overline{D_c}$.

Results of fracture prediction based on FEA simulations are listed in Table 2, where d_0 is the initial diameter of the specimen, d_f and d_p are the measured and predicted diameters at fracture, ε_{af} and ε_{ap} are

the measured and predicted accumulated engineering strain at fracture. Calculations of d_p/d_f, $(d_0-d_p)/(d_0-d_f)$ and $\varepsilon_{ap}/\varepsilon_{af}$ are also listed in the table. The cycle number followed by '+' indicates that fracture occurs when pulling the specimen after undergoing the indicated number of loading cycle. For monotonic tension tests, comparisons are made based on the test and predicted diameter at fracture, d_p/d_f and $(d_0-d_p)/(d_0-d_f)$. However for cyclic tests, the cycle number at fracture can be a more important measurement than the diameter at fracture since the change in the diameter is small within the loading cycle. The ratio of predicted and measured accumulated engineering strain at fracture is also a good measurement for both monotonic tension and cyclic tests for notched specimens. Overall, the criterion can reasonably predict the instance of fracture of the specimen using one set of material model parameters in numerical simulations of monotonic and cyclic tests. Ratios of $(d_0-d_p)/(d_0-d_f)$ for monotonic tests and $\varepsilon_{ap}/\varepsilon_{af}$ for cyclic tests are within 10% of unity except for three specimens that are within 15%.

6 Conclusions

The following conclusions can be drawn from the presented study:

1. A systematic procedure that enables the calculation of the parameters for the material model that are equally applicable for monotonic and cyclic loading has been developed.
2. Numerical simulations with the calibrated parameters have been found to be in good agreement with the measured stress-strain curves of the round specimen tests.
3. Good agreement has also been found between the test and predicted instance of fracture of the specimen using a variation of the continuum damage mechanics fracture criteria by Lemaitre using one set of material model parameters.

7 Acknowledgement

Financial support for this project was provided by the Natural Science and Engineering Research Council of Canada and Steel Structures Education Foundation.

8 References

ABAQUS (Simulia 2009). ABAQUS Version 6.9 Standard User's Manual. Dassault Systèmes Simulia Corporation, Providence, Rhode Island, USA.

Armstrong, P. J. and Frederick, C. O. (1966). A Mathematical Representation of the Multiaxial Bauschinger Effect. CEGB Report, RD/B/N/731, Berkeley Nuclear Laboratories, R&D Department, California, USA

Chaboche, J. L. (1986). Time-Independent Constitutive Theories for Cyclic Plasticity. International Journal of Plasticity, 2(2): 149-188.

Chen, J. (2010). An Experimental Study of Strain Rate Effects on Mild Steel. Master Thesis, Carleton University, Ottawa, Ontario, Canada.

Chinh, N. Q., Horvath, G., Horita, Z. and Langdon, T. G. (2004). A New Constitutive Relationship for the Homogeneous Deformation of Metals over a Wide Range of Strain. Acta Materialia, 52(12): 3555-3563.

Huang, Y. and Mahin, S. A. (2008). Evaluation of Steel Structure Deterioration with Cyclic Damaged Plasticity. The 14th World Conference on Earthquake Engineering, Beijing, China

Kanvinde, A. M. and Deierlein, G. G. (2004). Micromechanical Simulation of Earthquake-Induced Fracture in Steel Structures. Technical Report 145, John A. Blume Earthquake Engineering Center, Stanford University, California, USA.

Lemaitre, J. (1985). A Continuous Damage Mechanics Model for Ductile Fracture. Journal of Engineering Materials and Technology, 107(1): 83-89.

Wen, Z. (2012). Modelling of Ductile Fracture in Steel Structures for Monotonic and Cyclic Loading. Ph.D. Thesis, Carleton University, Ottawa, Ontario, Canada.